

# A UNIVERSAL DECLINE LAW OF CLASSICAL NOVAE. IV. V838 HER (1991): A VERY MASSIVE WHITE DWARF

MARIKO KATO

Department of Astronomy, Keio University, Hiyoshi, Yokohama 223-8521, Japan

IZUMI HACHISU

Department of Earth Science and Astronomy, College of Arts and Sciences, University of Tokyo, Komaba, Meguro-ku, Tokyo 153-8902, Japan

AND

ANGELO CASSATELLA

INAF, Istituto di Fisica dello Spazio Interplanetario, Via del Fosso del Cavaliere 100, 00133 Roma, Italy  
Departamento de Astrofísica, Facultad de Física, Universidad Complutense de Madrid, 28040 Madrid, Spain and  
Dipartimento di Fisica E. Amaldi, Università degli Studi Roma Tre, Via della Vasca Navale 84, 00146 Roma, Italy  
*to appear in the Astrophysical Journal*

## ABSTRACT

We present a unified model of optical and ultraviolet (UV) light curves for one of the fastest classical novae, V838 Herculis (Nova Herculis 1991), and estimate its white dwarf (WD) mass. Based on an optically thick wind theory of nova outbursts, we model the optical light curves with free-free emission and the UV 1455 Å light curves with blackbody emission. Our models of  $1.35 \pm 0.02 M_{\odot}$  WD reproduce simultaneously the optical and UV 1455 Å observations. The mass lost by the wind is  $\Delta M_{\text{wind}} \sim 2 \times 10^{-6} M_{\odot}$ . We provide new determinations of the reddening,  $E(B - V) = 0.53 \pm 0.05$ , and of the distance,  $2.7 \pm 0.5$  kpc.

*Subject headings:* — nova, cataclysmic variables — stars: individual (V838 Herculis) — stars: mass loss — ultraviolet: stars — white dwarfs

## 1. INTRODUCTION

V838 Her was discovered independently by Sugano (1991) on 1991 March 24.78 UT at 5.4 mag and by Alcock (1991) at  $\sim 5$  mag on 1991 March 25.67 UT. Alcock's visual discovery around the peak was made in strong twilight, so the peak magnitude was not accurate. The outburst time can be estimated from the upper limit (9 mag) pre-discovery observation by Ueta (1991) on JD 2,448,339.9 and Sugano's discovery on JD 2,448,340.281. In the present work we adopt the outburst time JD 2,448,340.0 as day zero and the maximum magnitude  $m_{V,\text{max}} = 5.4$  mag.

Soon after the optical maximum, the nova entered a very rapid decline phase, followed by a slight oscillatory behavior enduring several days and, later on, by a smooth decline. Infrared (IR) fluxes also showed a rapid decline, reaching a local minimum on day 6, followed by a rapid brightening. The spectral energy distribution was consistent with free-free emission from day 1.3 to 6.5, and thereafter with blackbody emission, ascribed to the formation of a hot dust shell (Chandrasekhar et al. 1992; Harrison & Stringfellow 1994; Kidger & Martinez-Roger 1993; Woodward et al. 1992). Indication of IR emission from silicate grains was reported only at a later phase (Lynch et al. 1992; Smith et al. 1995). Smith et al. (1995) suggested that silicate emission was due to a light echo by cold silicate grains deposited in a previous nova eruption.

Red and blue pre-outburst magnitudes were estimated

from the Palomar Sky Survey plates as 19 and 17.5, respectively, by West (1991), and 20.6 and 18.25 by Humphreys et al. (1991), but were contaminated by a closeby ( $\sim 1''$ ) star of similar magnitude. V838 Her returned to the pre-outburst magnitude  $V = 19.0$  on day 403, and  $V = 19.2$  on day 572 (Szkody & Ingram 1994).

In this series of papers, we have applied our universal decline law to many novae, including moderately fast novae (e.g., V1668 Cyg in Hachisu & Kato (2006) [hereafter referred as Paper I]) and a slow nova (GQ Mus in Hachisu et al. (2008) [Paper III]), and have succeeded in reproducing simultaneously optical, infrared, ultraviolet (UV) 1455 Å, and supersoft X-ray light curves. V838 Her is, however, one of the fastest classical novae, so it is interesting to see if the universal decline law also applied to such an extreme object. The main observational features of V838 Her are summarized in Tables 1 and 2. Section 2 reviews our observational results based on the *IUE* spectra. Our model light curves are briefly introduced in Section 3. The results of light curve fitting are given in Section 4. Discussions and conclusions follow in Sections 5 and 6. In Appendix we give several examples of nova light curves, which show high degree of homology, as predicted by our models.

## 2. UV OBSERVATIONS

V838 Her has been monitored by *IUE* from day 2 to day 831, mainly at low resolution. A gallery of UV spectra can be found in Cassatella et al. (2004a) and Vanlandingham et al. (1996).

In the following we revisit the problem of color excess  $E(B - V)$  of V838 Her, and describe the long term evolution of UV continuum and of emission lines. The UV

Electronic address: mariko@educ.cc.keio.ac.jp  
Electronic address: hachisu@ea.c.u-tokyo.ac.jp  
Electronic address: cassatella@fis.uniroma3.it

TABLE 1  
OBSERVATIONAL PROPERTIES OF V838 HERCULIS

subject		data	reference
discovery	...	JD 2,448,340.28	Sugano (1991)
nova speed class	...	very fast	
IR minimum	...	JD 2,448,345.94 (day 6)	
$t_3$	...	5.3-6 days	Harrison & Stringfellow (1994)
$m_{v,\max}$	...	5.4 mag	Sugano (1991)
$M_{V,\max}$ from $t_3$	...	-9.94 ~ -9.80 mag	equation (3)
distance	...	2.8-10 kpc	Vanlandingham et al. (1996); Harrison & Stringfellow (1994)
distance	...	$2.7 \pm 0.5$ kpc	this work
FWHM of UV 1455 Å	...	4.7 days	this work
$E(B - V)$	...	0.3-0.6	Vanlandingham et al. (1996); Harrison & Stringfellow (1994)
$E(B - V)$	...	$0.53 \pm 0.05$	this work
dust	...	very thin	see §5.2
orbital period	...	7.14 hr	Ingram et al. (1992); Leibowitz et al. (1992)
H-burning phase	...	< 1 yr	Szkody & Hoard (1994)

TABLE 2  
CHEMICAL ABUNDANCE BY WEIGHT

object	$X$	$Y$	$CNO$	$Ne$	$Na - Fe$	reference
Sun	0.7068	0.274	0.014	0.0018	0.0034	Grevesse & Anders (1989)
V838 Her	0.78	0.10	0.041	0.081	0.003	Vanlandingham et al. (1996)
V838 Her	0.59	0.31	0.030	0.067	0.003	Vanlandingham et al. (1997)
V838 Her	0.562	0.314	0.038	0.070	0.015	Schwarz et al. (2007)

spectra were retrieved from the *IUE* archive through the INES (*IUE* Newly Extracted Spectra) system<sup>1</sup>, which also provides full details of the observations. The use of the *IUE* INES data is particularly important for the determination of reddening correction because of the implementation of upgraded spectral extraction and flux calibration procedures compared to the previously published UV spectra.

### 2.1. Reddening Correction

As summarized by Vanlandingham et al. (1996), the color excess of V838 Her has been determined by several authors using different methods, based on the Balmer decrement (Ingram et al. 1992; Vanlandingham et al. 1996), the equivalent width of the Na I interstellar lines (Lynch et al. 1992), the ratio of the UV flux above and below 2000 Å (Starrfield et al. 1992), and the assumed intrinsic color at maximum light (Woodward et al. 1992). The mean value of these determinations, assuming to have the same weight, is  $E(B - V) = 0.50 \pm 0.12$ . Such a large error would cause large uncertainties on the distance and hence on the intrinsic parameters of the nova, as derived through a comparison with our models. This has driven us to revisit the problem of the reddening using an independent method that we consider more reliable than the previous ones, because of relying directly on its best detectable effect, i.e. the strength and shape of the 2175 Å broad dust absorption band.

The Galactic extinction curve (Seaton 1979) shows a pronounced broad maximum around 2175 Å due to dust absorption. Since it takes the same value  $X(\lambda) = A(\lambda)/E(B - V) \approx 8$  at  $\lambda = 1512, 1878, \text{ and } 2386$  Å, the slope of the straight line passing through the continuum points at these wavelengths is insensitive to  $E(B - V)$

in a  $(\lambda, \log F_\lambda)$  plot. This circumstance can be used to get a reliable estimate of  $E(B - V)$  as that in which the stellar continuum becomes closely linear in the 1512–2386 Å region, and passes through the continuum points at the above wavelengths. From 8 pairs of short and long wavelength *IUE* spectra taken from day 6 to day 69, i.e. during or close to the nebular phase, we have in this way found  $E(B - V) = 0.53 \pm 0.05$ , a value that we adopt in the following. Examples of *IUE* spectra of V838 Her corrected with  $E(B - V) = 0.53$  are reported in Figure 1 for day 10, 12, 15 and 22.

In principle, we could have estimated the  $E(B - V)$  color excess also from the observed relative intensities of the He II 1640 Å Balmer line, and the 2734 and 3203 Å Paschen recombination lines, compared with theoretical ratios, as done, for example in the case of GQ Mus (Paper III). Such lines were however too faint to be measured accurately.

### 2.2. Evolution of the UV Continuum

We have measured the mean flux in two narrow bands 20 Å wide centered at 1455 Å and 2855 Å, selected to best represent the UV continuum because little affected by emission lines (Cassatella et al. 2002). Figure 2 shows the time evolution of the  $F(1455 \text{ Å})$  and  $F(2885 \text{ Å})$  fluxes and of the UV color index  $C(1455 - 2885) = -2.5 \log[F(1455 \text{ Å})/F(2885 \text{ Å})]$ . The measurements were made on well exposed low resolution large aperture spectra. Figure 2 reports also, for comparison, the visual light curve obtained from the Fine Error Sensor (FES) counts on board *IUE*, once corrected for the time dependent sensitivity degradation (see Cassatella et al. 2004a, for details on the FES calibration).

It appears from Figure 2 that flux maximum is reached later in the UV 1455 Å band than in the 2885 Å and visual bands, as a result of the progressive shift of the

<sup>1</sup> <http://sdc.laeff.inta.es/ines/>

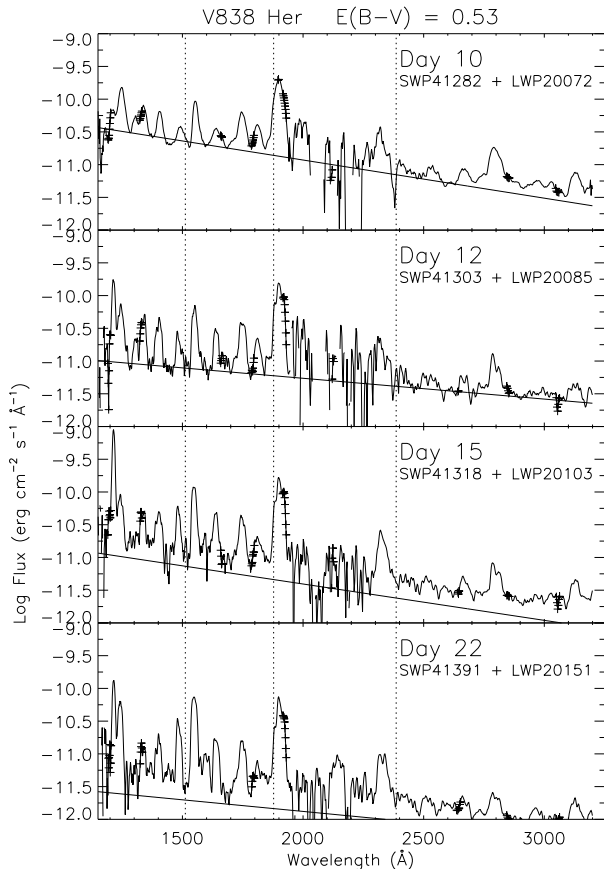


FIG. 1.— *IUE* spectra of V838 Her obtained at different dates (days after the outburst). The spectra have been corrected for reddening using  $E(B - V) = 0.53$ . The vertical dotted lines represent the wavelengths  $\lambda\lambda$  1512, 1878, and 2386 Å at which the extinction law takes the same value. With the adopted value of reddening, the stellar continuum underlying the many emission lines is well represented by a straight line all over the full spectral range. Saturated data points in the emission lines are labeled with pluses.

maximum emissivity towards shorter wavelengths. The progressive hardening of the UV spectrum stops after day 10, when the  $C(1455 - 2885)$  color index stabilizes around a value of zero. Both these features are a common property of the novae studied by Cassatella et al. (2002).

### 2.3. Evolution of the UV emission Lines

Figure 3 reports, as a function of time, the observed flux in the most prominent UV emission lines, as measured by us from the available *IUE* low resolution spectra. The figure shows that the maximum emission progressively shifts from low to high ionization lines, such that Mg II 2800 Å is the first to reach maximum, followed by C II 1335 Å, O I 1300 Å, C III] 1909 Å, N IV] 1487 Å, and N V 1240 Å maximum. The time delay of maximum emission  $\Delta t$  with respect to the visual maximum does in fact increase with increasing the line ionization potential  $\chi$  [eV], as better shown in Figure 4 where  $\Delta t$ , once normalized to the  $t_3$  time, is plotted as a function of  $\chi$  for the different emission lines. Here,  $t_3$  is the time in which the visual magnitude drops by 3 magnitudes from the optical peak. Such a behavior is consistent with that observed in a sample of seven CO novae, whose mean data from Cassatella et al. (2005) are over-

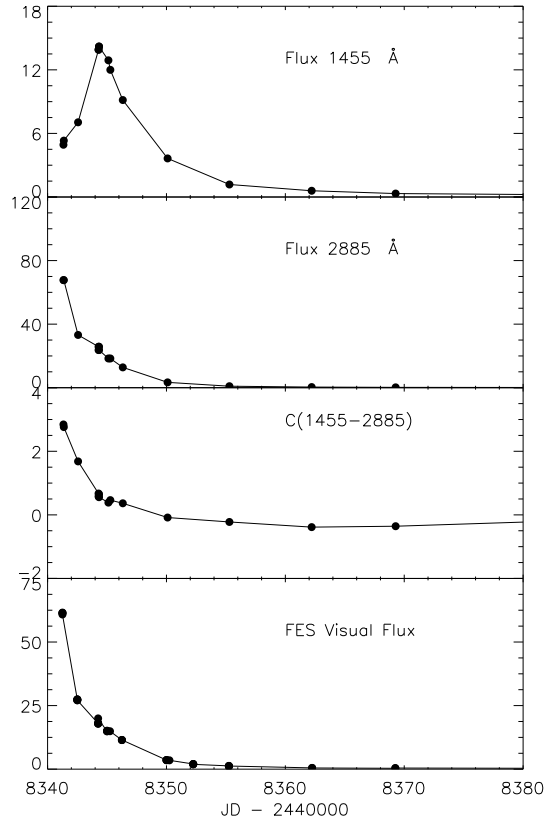


FIG. 2.— Evolution of the continuum fluxes at 1455 Å and 2885 Å, of the ultraviolet color index  $C(1455 - 2885)$ , and of the  $V_{\text{FES}}$  visual flux of V838 Her. Fluxes are in units of  $10^{-13} \text{ erg cm}^{-2} \text{ s}^{-1} \text{ \AA}^{-1}$ , not corrected for reddening. Only the color index has been corrected for reddening using  $E(B - V) = 0.53$ .

plotted for comparison. In particular, note that the maximum emission in C III] 1909 Å and N III] 1750 Å takes place after a time of  $\Delta t/t_3 \approx 2$ , as in CO novae. This time has been identified in Cassatella et al. as the start of the pre-nebular phase.

### 2.4. High Resolution Emission Line Profiles

Good quality *IUE* high resolution spectra of V838 Her are available only at two dates: day 2.5 (LWP 19993) and day 15 (SWP41317). The most prominent feature in the long wavelength spectrum of day 2.5 is the broad P Cygni profile of the Mg II 2800 Å doublet (Figure 5). A comparison with theoretical P Cygni profiles computed with the SEI (Sobolev Exact Integration) method (Lamers et al. 1987; Groenewegen & Lamers 1989) indicates that the terminal velocity of the wind is  $\approx 3000 \text{ km s}^{-1}$ . The huge emission compared with the absorption component, usual in novae, is due to efficient population of the upper levels of the doublet by electron collisions.

Another interesting line profile is that of the C III] 1906.68-1908.73 Å doublet shown in Figure 6, which is the strongest emission line observed in the short wavelength spectrum of day 15. As it appears from the figure, the C III] emission has a very complex profile. One way to interpret this profile is that the emitting region is very inhomogeneous in terms of density and velocity

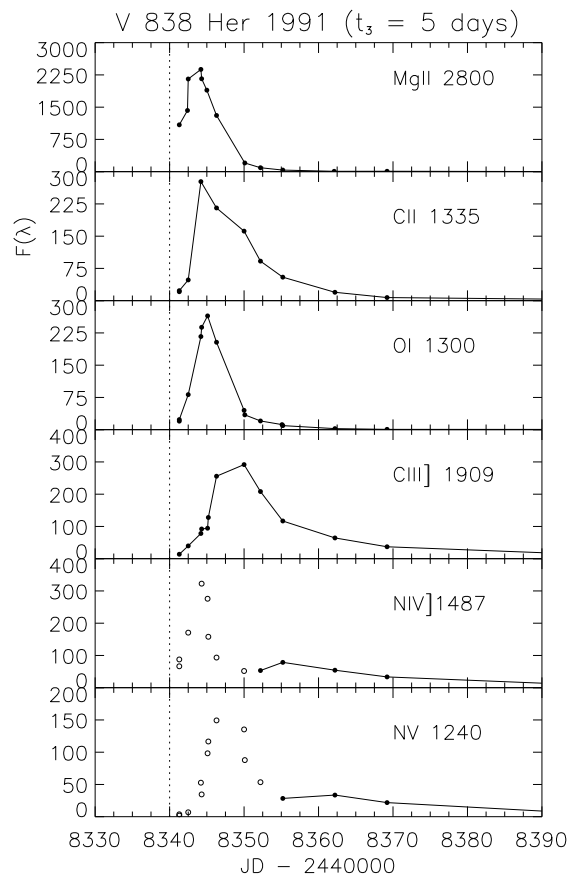


FIG. 3.— Evolution of the observed fluxes in the most prominent emission lines of V838 Her, in units of  $10^{-12}$  erg  $\text{cm}^{-2}$   $\text{s}^{-1}$ . Open dots in the N IV] and N V panels refer to features not due to these transitions.

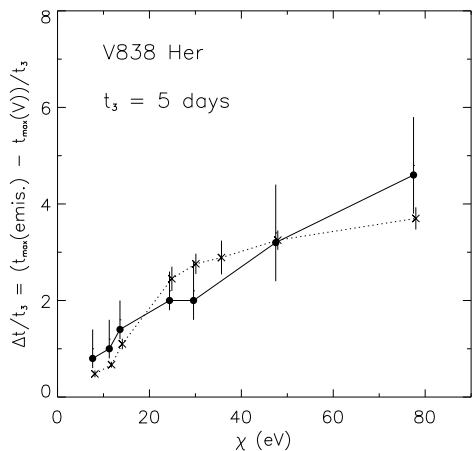


FIG. 4.— Delay of the flux maximum of the emission lines, normalized to the  $t_3$  time, as a function of the corresponding ionization potential for V838 Her (filled circles). The emission lines considered, in order of increasing ionization potential, are: Mg II 2800 Å, C II 1335 Å, O I 1300 Å, C III] 1909 Å, N III] 1750 Å, N IV] 1487 Å, and N V 1240 Å. We also show, for comparison, the average values of CO novae (crosses) in Cassatella et al. (2005). In this case, the x-axis has been shifted by 0.5 eV to make the error bars visible and the O III 1660 Å line is added between the N III] and N IV] lines.

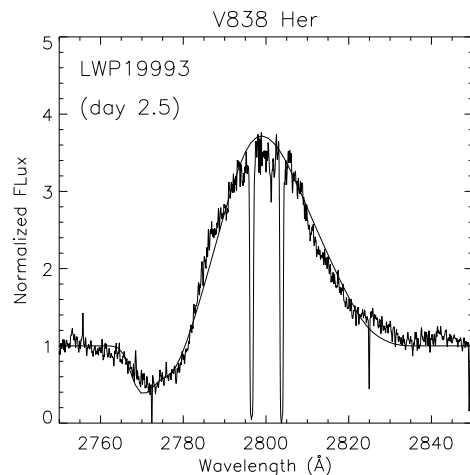


FIG. 5.— P Cygni profile of the Mg II 2800 Å doublet from the IUE spectrum LWP19993 of V838 Her taken on day 2.5. The observed profiles have been fitted with a theoretical P Cygni profile, obtained through the SEI method (Lamers et al. 1987; Groenewegen & Lamers 1989), indicated as a thick line. The derived wind terminal velocity is  $\approx 3000$   $\text{km s}^{-1}$ . Fluxes are normalized to the local continuum. Note the presence of the narrow interstellar components of the doublet at about the laboratory wavelength.

structure. This possibility cannot be ruled out a priori also in view of the presence of complex emission line profiles, e.g., in the hydrogen Balmer lines (see Iijima et al. 2009). The other possibility is that the C III] emission is eroded by overlying absorption from an outer shell. A likely source of overlying absorption is the principal and diffuse absorption components from the Fe III UV 34 triplet at radial velocity of  $-500$   $\text{km s}^{-1}$  and  $-1600$   $\text{km s}^{-1}$ , respectively. Such components have already been confidently identified to affect the C III] emission line in V1974 Cyg (Cassatella et al. 2004b).

### 3. THE MODEL OF NOVA LIGHT CURVES

In this and previous papers, we have presented a unified model for the IR, optical, UV, and supersoft X-ray light curves of several classical novae. Our models are based on the optically thick wind theory of nova outbursts as described in Kato & Hachisu (1994) and in Paper I.

#### 3.1. Optically Thick Wind Model

After a thermonuclear runaway sets in, the photosphere of the white dwarf (WD) envelope expands greatly to a giant size with  $R_{\text{ph}} \gtrsim 100 R_{\odot}$ . The envelope settles into steady-state around the optical peak. The following decay phase can be described by a sequence of steady state solutions (e.g., Kato & Hachisu 1994). Using the same method and numerical techniques as in Kato & Hachisu (1994), we have followed the evolution of novae by connecting steady state solutions along the decreasing envelope mass sequence.

The equations of motion, radiative diffusion, and conservation of energy, are solved from the bottom of the hydrogen-rich envelope through the photosphere, under the condition that the solution goes through a critical point of a steady-state wind. The winds are accelerated deep inside the photosphere so that they are called “optically thick winds.” We have used updated OPAL opaci-

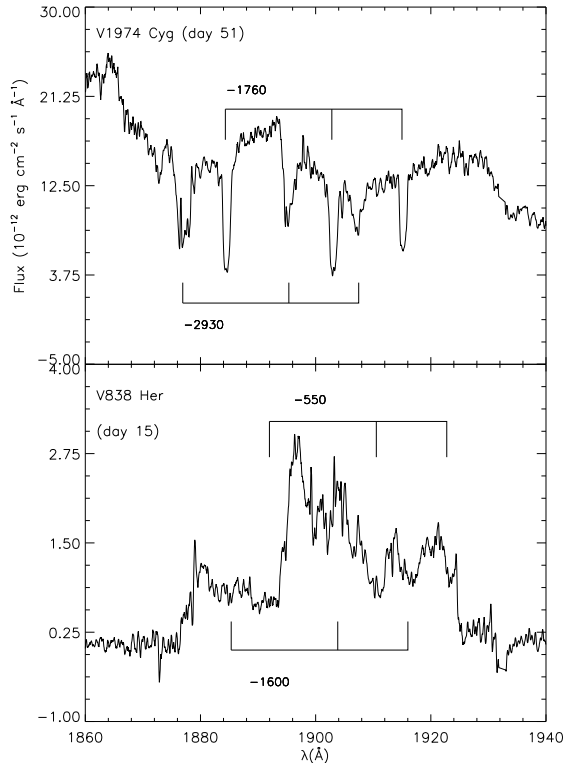


FIG. 6.— Spectra of V838 Her and V1974 Cyg around 1900 Å. In the case of V838 Her, a strong emission line from the C III] 1907-1909 Å doublet is present and appears eroded by overlying absorption from the principal and diffuse system components of the Fe III UV 34 multiplet. On day 15, these components are seen at  $-550 \text{ km s}^{-1}$  and  $-1600 \text{ km s}^{-1}$ , respectively. In V1974 Cyg, the C III] doublet emission is not present yet (it will appear at a later stage), but it is easy to appreciate the presence of the principal and diffuse absorption components of the Fe III UV 34 multiplet at  $-1760 \text{ km s}^{-1}$  and  $-2930 \text{ km s}^{-1}$ .

ties (Iglesias & Rogers 1996). Optically thick winds stop after a large part of the envelope is blown in the wind. As one of the boundary conditions for our numerical code, we assume that photons are emitted at the photosphere as a blackbody with a photospheric temperature  $T_{\text{ph}}$ .

The UV 1455 Å flux is estimated directly from blackbody emission instead of modeling WD atmosphere. This approximation is reasonably accurate in a very narrow wavelength range around UV 1455 Å flux (Cassatella et al. 2002, and paper III) near its peak. Infrared and optical fluxes are calculated from free-free emission by using physical values of our wind solutions. Physical properties of these wind solutions are given in our previous papers (Hachisu et al. 1999a; Kato 1983, 1997, 1999; Kato & Hachisu 1994).

We neglect helium ash layer which may develop underneath the hydrogen burning zone in mass increasing WDs as in RS Oph (see Hachisu et al. 2007). We suppose that the WD mass is decreasing in V838 Her, because metal enhancement is observed in V838 Her (see Table 2). Metal enrichment is an indicator of decreasing WD mass (e.g., Prialnik 1986; Prialnik & Kovetz 1995).

### 3.2. Multiwavelength Light Curves

In the optically thick wind model, a large part of the envelope is ejected continuously for a relatively long

period (e.g., Kato & Hachisu 1994). After maximum expansion of the photosphere, the photospheric radius ( $R_{\text{ph}}$ ) gradually decreases keeping the total luminosity ( $L_{\text{ph}}$ ) almost constant. The photospheric temperature ( $T_{\text{ph}}$ ) increases with time because  $L_{\text{ph}} = 4\pi R_{\text{ph}}^2 \sigma T_{\text{ph}}^4$ . The maximum emission shifts from optical to supersoft X-ray through UV and extreme ultraviolet. This causes the optical luminosity to decrease and the UV luminosity to increase with a timescale that depends strongly on the WD mass and weakly on the chemical composition of the envelope (e.g. Kato 1997, Paper I).

### 3.3. Universal Decline Law of Free-Free Light Curves

We calculated the optical and IR fluxes of free-free emission outside the photosphere of optically thick winds by

$$F_{\nu} \propto \int N_e N_i dV \propto \int_{R_{\text{ph}}}^{\infty} \frac{\dot{M}_{\text{wind}}^2}{v_{\text{wind}}^2 r^4} r^2 dr \propto \frac{\dot{M}_{\text{wind}}^2}{v_{\text{ph}}^2 R_{\text{ph}}}, \quad (1)$$

(see Paper I for more details), where  $F_{\nu}$  is the flux at the frequency  $\nu$ ,  $N_e$  and  $N_i$  are the number densities of electrons and ions, respectively,  $V$  is the emitting volume,  $R_{\text{ph}}$  is the photospheric radius,  $\dot{M}_{\text{wind}}$  is the wind mass loss rate, and  $v_{\text{ph}}$  is the velocity at the photosphere. We also assume that  $N_e \propto \rho_{\text{wind}}$ ,  $N_i \propto \rho_{\text{wind}}$ , and use the continuity equation, i.e.,  $\rho_{\text{wind}} = \dot{M}_{\text{wind}}/4\pi r^2 v_{\text{wind}}$ , where  $\rho_{\text{wind}}$  and  $v_{\text{wind}}$  are the density and velocity of the wind, respectively. Finally, we assume that  $v_{\text{wind}} = \text{const.} = v_{\text{ph}}$  outside the photosphere.

This equation has successfully reproduced the optical and infrared light curves of several novae in outburst (see papers of this series; Hachisu & Kato 2006, 2009; Kato et al. 2008). In the case of V838 Her, the early decay (until day 6) of  $J$ ,  $H$ , and  $K$ -bands are almost parallel to each other as shown later in Figure 8, whereas  $J$  is not shown for clarity; This is one of the characteristic properties of free-free emission (see Appendix of Paper III). Also the spectrum of V838 Her is consistent with that of free-free emission as mentioned in Section 1. Thus, we can safely apply our method to V838 Her.

After the optically thick wind stops, the total mass of the ejecta remains constant with time. The flux from such homologously expanding ejecta is

$$F_{\nu} \propto \int N_e N_i dV \propto \rho^2 V \propto \frac{M_{\text{ej}}^2}{V^2} V \propto R^{-3} \propto t^{-3}, \quad (2)$$

where  $\rho$  is the mean density, and  $M_{\text{ej}}$  is the ejecta mass. We assume that the ejecta are expanding at a constant velocity,  $v$ . So we have  $R = vt$ , where  $t$  is the time after the outburst. The proportionality constants in equations (1) and (2) cannot be determined a priori because radiative transfer is not calculated outside the photosphere; these were determined using the procedure described below.  $F_{\lambda}$  is also represented by equations (1) and (2), but the proportionality constant depends on wavelength since  $F_{\lambda} \propto \lambda^{-2} F_{\nu}$ .

If we assume an expanding shell with constant thickness, the flux is proportional to  $F_{\nu} \propto t^{-2}$  as discussed in V723 Cas (Evans et al. 2003). In V1500 Cyg and V1974 Cyg, however, we found that the flux decline rate can be well represented by  $t^{-3}$  (see Paper I). As we will

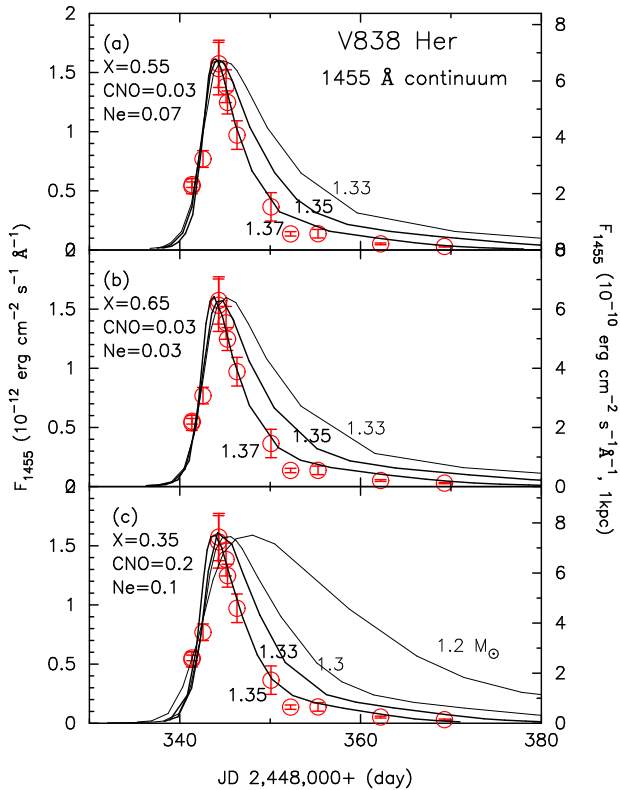


FIG. 7.— UV 1455 Å light curve-fitting for V838 Her. Large open circles with error bar: observed UV 1455 Å flux and root mean square of errors (units of the left-hand-side axis). Three different sets of chemical composition are assumed. (a)  $X = 0.55$ ,  $X_{\text{CNO}} = 0.03$ ,  $X_{\text{Ne}} = 0.07$ , and  $Z = 0.02$ , (b)  $X = 0.65$ ,  $X_{\text{CNO}} = 0.03$ ,  $X_{\text{Ne}} = 0.03$ , and  $Z = 0.02$  and (c)  $X = 0.35$ ,  $X_{\text{CNO}} = 0.2$ ,  $X_{\text{Ne}} = 0.1$ , and  $Z = 0.02$ . The WD mass is attached to each light curve. Theoretical flux  $F_{1455}$  is presented for an arbitrarily assumed distance of 1.0 kpc and no absorption (the scale in the right-hand-side is for  $1.37M_{\odot}$  in (a) and (b), but for  $1.35M_{\odot}$  in (c). For other curves scales are normalized arbitrarily).

see later, the decline rate of V838 Her is consistent with  $t^{-3}$ .

As the proportional constant in equation (2) cannot be determined theoretically, and there is no representative timescale, this later part of the light curve does not contain any information on the WD mass. Therefore, we do not use this part in our light curve fitting.

### 3.4. System Parameters of Optically Thick Wind Model

The light curves of our optically thick wind model are parameterized by the WD mass ( $M_{\text{WD}}$ ), chemical composition of the envelope ( $X, Y, X_{\text{CNO}}, X_{\text{Ne}}, Z$ ), and the envelope mass ( $\Delta M_{\text{env},0}$ ) at the time of outburst (JD 2,448,340.0). Note that the metal abundance,  $Z$ , includes carbon, nitrogen, oxygen, and neon with solar composition ratios and that  $X_{\text{CNO}}$  and  $X_{\text{Ne}}$  denote additional excesses.

Table 2 summarizes the chemical abundance determinations so far available for V838 Her, as first provided by Vanlandingham et al. (1996), superseded by the later re-determinations by Vanlandingham et al. (1997), and extended by Schwarz et al. (2007) from spectra taken at four epochs (day 28, 60, 79 and 148). We thus assume the chemical composition of V838 Her to be  $X = 0.55$ ,  $Y = 0.33$ ,  $X_{\text{CNO}} = 0.03$ ,  $X_{\text{Ne}} = 0.07$ , and  $Z = 0.02$ . We call it the “standard” composition set. We also assumed

two other sets of composition for comparison. The first case is  $X = 0.65$ ,  $Y = 0.27$ ,  $X_{\text{CNO}} = 0.03$ ,  $X_{\text{Ne}} = 0.03$ , and  $Z = 0.02$ , expressing less enrichment of heavy elements such as in V382 Vel and QU Vul, and the second case is  $X = 0.35$ ,  $Y = 0.33$ ,  $X_{\text{CNO}} = 0.2$ ,  $X_{\text{Ne}} = 0.1$ , and  $Z = 0.02$  which may be an extreme case of metal enrichment for V838 Her but appropriate composition for V1974 Cyg and V351 Pup, although abundance estimates are very different among different authors (see Table 1 in Paper I which lists observational estimates of abundance of nova ejecta).

The latter two recent determinations both indicate an excess of helium with respect to hydrogen, i.e.,  $X/Y = 1.9$  (Vanlandingham et al. 1997) and 1.8 (Schwarz et al. 2007), against the solar value of  $0.7/0.28 = 2.58$ . In massive WDs about one tenth of hydrogen is consumed by nuclear burning to produce thermal and gravitational energy during the early phase of the outburst (Politano et al. 1995; Prialnik & Kovetz 1995). Supposing that  $\Delta X = 0.1$  of hydrogen is converted into helium, the hydrogen/helium ratio becomes  $X/Y = (0.7 - 0.1)/(0.28 + 0.1) = 1.6$ . If, in addition, a fraction 10% of the envelope mass is dredged up and mixed into the envelope, the above envelope composition is further changed to  $X = 0.545$ ,  $Y = 0.345$ , and  $X_{\text{CNO}} + X_{\text{Ne}} + Z = 0.11$ . This is very consistent with the observational results by Vanlandingham et al. (1997) and Schwarz et al. (2007) in Table 2.

## 4. LIGHT CURVE FITTING

We have searched for the model light curves that best fit the observational data among models with WD mass 1.2, 1.3, 1.33, 1.35, and 1.37  $M_{\odot}$ , for the three sets of chemical abundance quoted above. As shown in previous papers of this series, we have proven the light curve fitting method to be a powerful tool to obtain the intrinsic nova parameters. In particular, we have shown that the theoretical light curves of UV 1455 Å continuum are very sensitive to the WD mass, so that the WD mass can be determined with a good accuracy.

Figure 7 shows the fits to the UV 1455 Å light curve of V838 Her for three different chemical composition and various WD masses. Figure 7a) shows that  $M_{\text{WD}} = 1.37 M_{\odot}$  model is in a good agreement with the observed data but models of  $M_{\text{WD}} \leq 1.33 M_{\odot}$  produce too slow declines. Models of 1.2 and 1.3  $M_{\odot}$  are omitted because they are too slow to be compatible with the observation. Similar results are obtained if we increase the hydrogen content and decrease the heavy elements slightly to  $(X, X_{\text{CNO}}, X_{\text{Ne}}) = (0.65, 0.03, 0.03)$  as in Figure 7b. On the other hand, if we decrease the hydrogen and increase the heavy elements to  $X = 0.35$ ,  $X_{\text{CNO}} = 0.2$ , and  $X_{\text{Ne}} = 0.1$  (Figure 7c), which may be an extreme case for V838 Her, the  $1.35M_{\odot}$  model shows a good fitting and less massive WDs ( $M_{\text{WD}} \leq 1.3$ ) are probably excluded. Therefore, from the UV light curve fitting, we see that the WD in V838 Her is as massive as  $M_{\text{WD}} \geq 1.35 M_{\odot}$ .

Figure 8 reports the model fits to the visual and infrared light curves for the standard composition set. We have assumed that, at these wavelengths, the light curve is dominated by free-free emission (i.e., can be calculated from eq. [1]). Since its shape does not depend on wavelength, one can apply the same light curve model to the optical and IR data. Figure 8 shows indeed that, if suit-

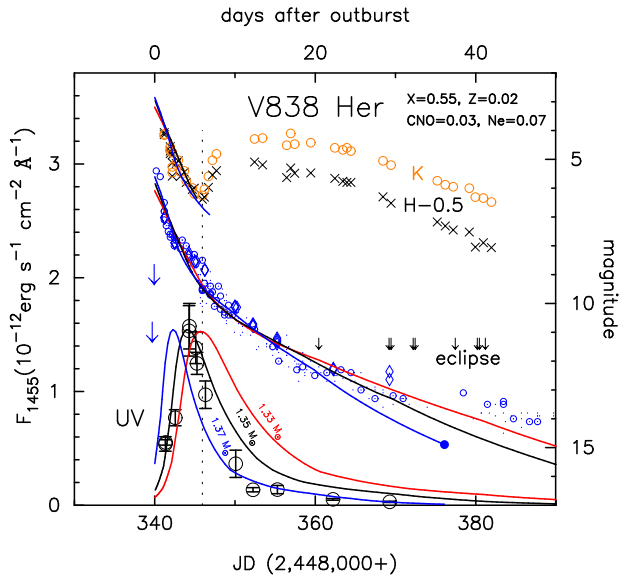


FIG. 8.— Theoretical and observed optical, infrared, and UV light curves of V838 Her. Theoretical light curves refer to models with  $M_{\text{WD}} = 1.37 M_{\odot}$  (blue),  $1.35 M_{\odot}$  (black), and  $1.33 M_{\odot}$  (red). Observed visual and V magnitudes are denoted by small open circles (IAU Circulars 5222, 5223, 5224, 5226, 5228, 5229, 5233, 5234, 5238, 5254 and 5265), and by diamonds (*IUE*  $V_{\text{FES}}$ : Cassatella et al. (2004a)). Two large downward arrows indicate optical upper limit observations from IAU Circular 5265. Small downward arrows denote the dates of eclipse minima reported by Leibowitz et al. (1992) and by Kato & Hirata (1991). Infrared data are taken from IAU Circulars 5223, 5224, 5228, 5230, 5232, 5236, 5246, 5254 and from Harrison & Stringfellow (1994).  $K$  and  $H$  magnitudes are denoted by middle-sized open circles and crosses, respectively.  $H$  magnitudes are shifted up by 0.5 mag. Large open circles denote the observed UV 1455 Å band flux (Cassatella et al. 2002, except one newly obtained point) in units of  $10^{-12} \text{ erg s}^{-1} \text{ cm}^{-2} \text{ Å}^{-1}$ . For theoretical UV curves, we assume the distance and absorption in Table 3 to fit the observational data. Vertical dotted line indicates the epoch of the IR minimum.

ably upward-shifted, the optical light curve also fits the infrared fluxes, at least until day 6, when an IR flux minimum was reached (indicated as a vertical dashed line in Figure 8), owing to thermal emission from dust (see Section 1 and Section 5).

Figure 9 provides, in logarithmic time, another view of the model fit to the data. This figure shows that, at very late phases, optical and infrared fluxes decay along with the  $F_{\lambda} \propto t^{-3}$  line as predicted from equation (2). This circumstance does not bring, however, any information on the WD mass. As shown in Figures 8 and 9, among models with the WD mass of 1.33, 1.35 and  $1.37 M_{\odot}$ , the  $1.35 M_{\odot}$  WD provides a best fit representation of the UV light curves as well as the optical and infrared light curves.

Figures 10 and 11 show the model fits for the other two sets of chemical composition. In Figure 10, we get the best fit models of  $1.35 M_{\odot}$  WD from fitting optical, IR and UV fluxes. In Figure 11, however, we cannot fit both of the UV and optical fluxes simultaneously. When we fit the optical, the model UV flux rises too earlier, and then we cannot obtain a good fit in the UV. This indicates that the assumed composition, i.e.,  $X = 0.35$ ,  $X_{\text{CNO}} = 0.2$ , and  $X_{\text{Ne}} = 0.1$  is too metal rich and not appropriate for V838 Her.

To summarize we may conclude that the WD mass is  $M_{\text{WD}} = 1.35 \pm 0.02 M_{\odot}$ . The model parameters and the

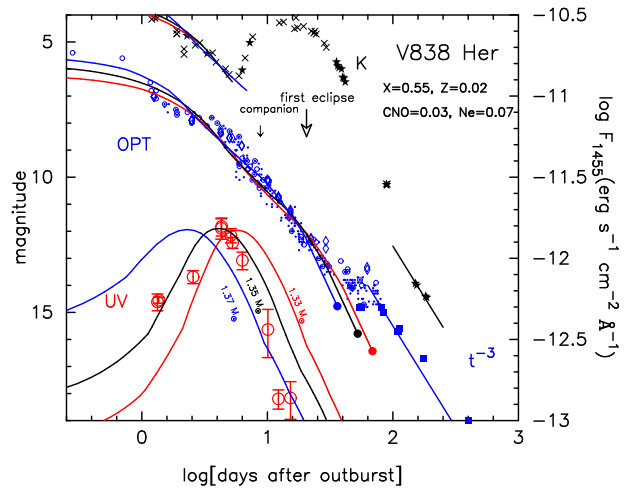


FIG. 9.— Same as Figure 8, but for logarithmic time. The AAVSO data (small dots) are plotted only until day 68, because after that time the nova becomes fainter than 14 mag, i.e., the brightness of a closeby star. The optical data for the late phases (filled squares) are taken from Ingram et al. (1992) and Szkody & Ingram (1994). The IR data denoted by the asterisk are taken from Harrison & Stringfellow (1994). The emergence time of companion for the  $1.35 M_{\odot}$  WD model (day 9) and the first eclipse observation (day 21) are also indicated by the small and large downward arrows.

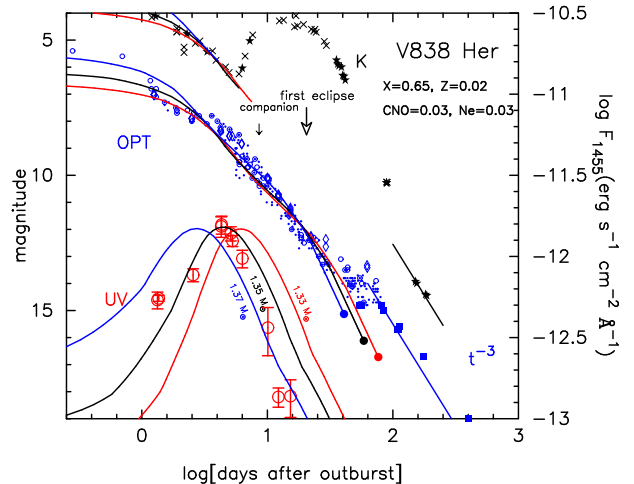


FIG. 10.— Same as Figure 9 but for theoretical model with the composition set of less enhancement of heavy elements, i.e.,  $X = 0.65$ ,  $X_{\text{CNO}} = 0.03$ , and  $X_{\text{Ne}} = 0.03$ .

main results are summarized in Table 3.

## 5. DISCUSSION

### 5.1. “Optical Drop” in Woodward et al. (1992)

Woodward et al. (1992) and Harrison & Stringfellow (1994) claimed that the rise of infrared fluxes starting on JD 2,448,346 (day 6) was accompanied by a sudden drop of the visual magnitude by  $\Delta V \sim 0.9$ . Woodward et al. (1992) proposed that the sudden drop of the visual flux was caused by an optically thick clump of matter ejected toward the earth on day 6 (indicated by the vertical dotted line in Figure 12). Afterwards, the optical flux continued to decline but at a substantially lower level than extrapolated from the light curve of previous days, shown by a dash-dotted line in Figure 12 (which mimics the dashed curve in Figure 1 of Woodward et al. 1992).

TABLE 3  
SUMMARY OF THE PRESENT MODEL

subject	units	model 1	model 2	model 3	model 4	model 5
		$1.37 M_{\odot}$	$1.35 M_{\odot}$	$1.33 M_{\odot}$	$1.35 M_{\odot}$	$1.33 M_{\odot}$
outburst day ( $t_0$ )	...	JD 2,448,340	←	←	←	←
$E(B - V)$	...	0.53	←	←	←	←
$X$	...	0.55	←	←	0.65	0.35
$Y$	...	0.33	←	←	0.27	0.33
$CNO$	...	0.03	←	←	0.03	0.2
$Ne$	...	0.07	←	←	0.03	0.1
$Z$	...	0.02	←	←	←	←
distance from UV fit	...	kpc 2.7	2.7	2.6	2.6	2.8
$M_{V,max}$ from UV fit	...	mag -8.41	-8.40	-8.32	-8.32	-8.48
WD envelope mass	...	$M_{\odot}$ $2.5 \times 10^{-6}$	$2.9 \times 10^{-6}$	$3.5 \times 10^{-6}$	$2.6 \times 10^{-6}$	$2.9 \times 10^{-6}$
mass lost by winds	...	$M_{\odot}$ $2.3 \times 10^{-6}$	$2.6 \times 10^{-6}$	$3.0 \times 10^{-6}$	$2.2 \times 10^{-6}$	$2.5 \times 10^{-6}$
wind phase	...	days 37	52	68	58	39
secondary mass	...	$M_{\odot}$ 0.76 <sup>a</sup>	←	←	←	←
separation	...	$R_{\odot}$ 2.4	2.4	2.4	2.4	2.4
$R_1^*$	...	$R_{\odot}$ 1.0	1.0	1.0	1.0	1.0
$R_2^*$	...	$R_{\odot}$ 0.8	0.8	0.8	0.8	0.8
companion's emergence	...	days 10	15	19	15	14

<sup>a</sup> estimated from eq. (10).

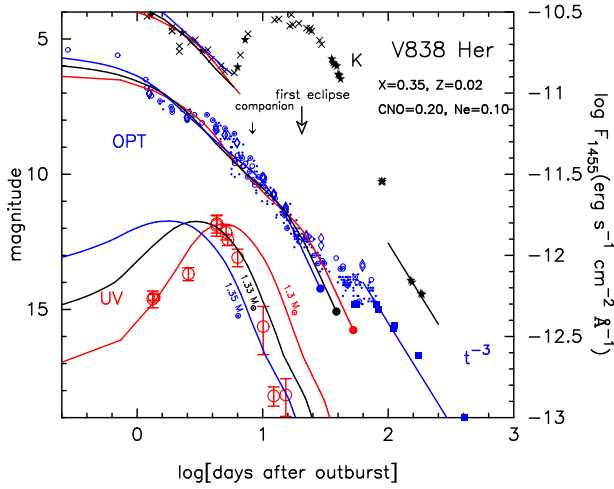


FIG. 11.— Same as Figure 9 but for theoretical model with the composition set of much enhancement of heavy elements, i.e.,  $X = 0.35$ ,  $X_{CNO} = 0.2$ , and  $X_{Ne} = 0.1$ .

The visual magnitudes used by Woodward et al. (1992) and by Harrison & Stringfellow (1994) were taken from IAU Circulars. These data were, however, obtained by different observers. We have tested self-consistency of the different sets by connecting the data obtained by the same observer (Figure 12). It clearly appears from the figure that there are systematic differences between the data sets from different observers, and also that no observer reported the sudden drop at JD 2,448,346, in agreement with the smooth decline shown by the homogeneous set of the  $IUE V_{FES}$  magnitudes, also given in the same figure. Moreover, the magnitudes corresponding to just before and after the sudden drop are 8.5 mag at Mar. 30.46 UT and 9.54 mag at Mar. 30.466 UT, respectively, which are obtained by different observers. If we take the reported observation time as a three-digit number, the magnitude should dropped by 0.006 day = 8.6 minutes. This is too short to have some significant change in stellar luminosity. Therefore, we conclude that the claimed  $V$  magnitude drop is an artifact caused by connecting the different data set with systematic difference.

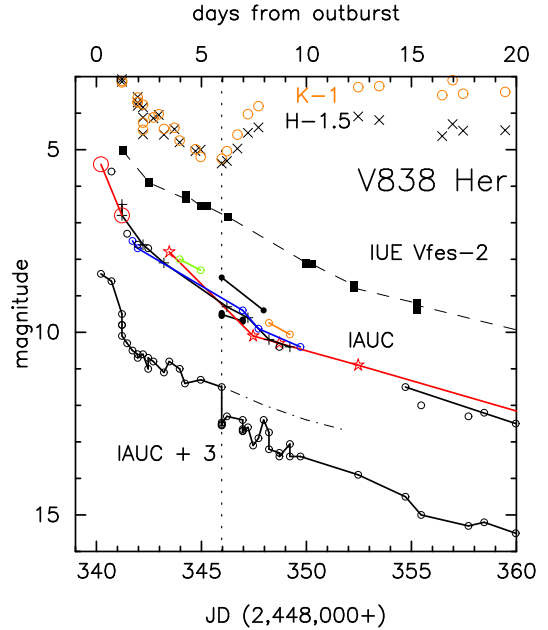


FIG. 12.— Optical and infrared light curves. The optical data are shown separately to assess their homogeneity. From bottom to top, IAUC+3: data from IAU Circulars, shifted by 3 mag downward, in which all the data are connected along the reported observing time. IAUC: same data of IAU Circulars but are connected between points only obtained by the same observer.  $IUE V_{FES} - 2$ :  $IUE V_{FES}$  data connected by a dashed line (shifted 2 mag upward).  $K - 1$  and  $H - 1.5$ : infrared  $K$  and  $H$  data, shifted by 1.0 and 1.5 mag upward, respectively. The time of the “drop in optical magnitude” proposed by Woodward et al. (1992) is indicated with a vertical dashed line, and their “unabsorbed light curve” with a dot-dashed line.

Should the 0.9 mag optical drop be real and due to dust absorption from a clump of matter ejected along the line of sight, one would expect to observe a simultaneous strong absorption of the UV flux. The decrease in the UV flux is estimated to be a factor of  $10^{(8.3/3.1) \times 0.9} = 257$ . Figure 8 shows, however, no indication of such a drastic decrease in the UV flux.

## 5.2. Dust Formation: Comparison with V1668 Cyg

After the local minimum on day 6, the IR fluxes increased to reach a local maximum around day 12 (in  $H$  band), being ascribed to thermal emission from an optically thin dust shell (Chandrasekhar et al. 1992; Woodward et al. 1992; Kidger & Martinez-Roger 1993; Harrison & Stringfellow 1994). As shown in Figure 8, however, there is no clear evidence for a corresponding decrease in the UV fluxes. In this subsection we make a comparison with nova V1668 Cyg in order to understand to what extent dust absorption can cause significant effects on the UV and optical fluxes in the case of V838 Her.

V1668 Cyg is a well studied moderately fast nova. It developed an optically thin dust shell giving rise to the infrared second maximum  $\sim 60$  days after the optical peak (Stickland et al. 1981). In correspondence to the second IR maximum, the UV 1455 Å flux suddenly dropped by  $1/2 \sim 1/3$  of what expected from a linear decline law (Kato & Hachisu 2007). The evolution of V1668 Cyg ( $t_3 \sim 23$  days) was much slower than that of V838 Her, due to its smaller WD mass ( $\sim 0.95 M_\odot$ , see Paper I). Consequently, the ejected mass of V1668 Cyg is expected to be much larger than that of V838 Her. Namely, since the ejected mass of V1668 Cyg is estimated to be  $5.8 \times 10^{-5} M_\odot$  (Kato & Hachisu 2007), while we estimate that it was  $2 - 3 \times 10^{-6} M_\odot$  for V838 Her from our best fit models (see Table 3). One should thus expect that the dust mass of V838 Her was roughly ten times smaller.

Observationally, Gehrz et al. (1980) estimated for V1668 Cyg the mass of dust (condensed carbon) to be  $2.5 \times 10^{-8} M_\odot$  and shell mass of hydrogen to be  $2 \times 10^{-5} M_\odot$ , which is consistent with the above value of total ejecta mass  $5.8 \times 10^{-5} M_\odot$ .

Also, Chandrasekhar et al. (1992) estimated the total grain mass of V838 Her to be  $1.6 \times 10^{-8} M_\odot$  assuming distance of  $d = 8.3$  kpc. As the mass estimate is proportional to  $d^2$ , where  $d$  is the distance to the star, this corresponds to  $1.7 \times 10^{-9} M_\odot$  for  $d = 2.7$  kpc here adopted (see Section 5.3 below). Harrison & Stringfellow (1994) estimated the dust mass of V838 Her to be  $1.1 \times 10^{-8} M_\odot$  at dust shell maximum for  $d = 5.5$  kpc, which is proportional to the IR luminosity, therefore, a smaller value  $2.7 \times 10^{-9} M_\odot$  is derived for  $d = 2.7$  kpc.

In any case, the dust mass of V838 Her appears to be one tenth of dust mass of V1668 Cyg, a value that is not expected to affect significantly the UV fluxes even at the time of the second infrared maximum, explaining then the absence of any quick drop in the UV 1455 Å light curve.

### 5.3. Distance

The interstellar extinction and the distance were estimated with various methods (Harrison & Stringfellow 1994; Vanlandingham et al. 1996, for summary), the values of which are largely scattered as  $E(B - V) = 0.3 - 0.6$  and  $d = 2.8 - 10$  kpc (see Table 1). One of the typical way to estimate the distance is to use  $t_3$  time or using statistical properties such as a given magnitude at a certain stage of light curve.

Let us begin with the distance estimate using the Maximum Magnitude versus Rate of Decline (MMRD) law. The absolute  $V$  magnitude at maximum  $M_{V,\max}$  can

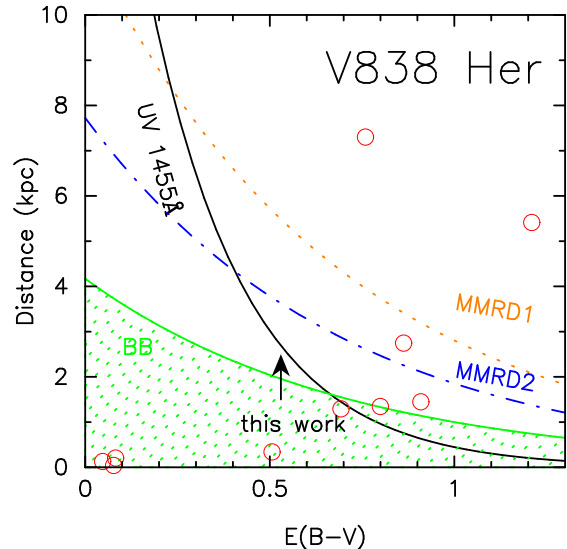


FIG. 13.— Distance-reddening relations for V838 Her. Solid line labeled “UV 1455 Å” (see Eq. [8]), corresponds to our best fit model  $M_{\text{WD}} = 1.35 M_\odot$ . Dotted curve represents the maximum magnitude vs. rate of decline relation calculated from Schmidt-Kaler’s law, with  $t_3 = 5.3$  days (labeled “MMRD1”, eq. [5]); the dash-dotted curve shows another MMRD relation, by Della Valle & Livio (1995), with  $t_2 = 1.4$  day (labeled “MMRD2”, eq. [7]). “BB” is the line of eq.(9). An arrow indicates our reddening determination  $E(B - V) = 0.53$ . Open circles denote nearby stars’ distance vs.  $E(B - V)$  (taken from (46/2) in Neckel & Klare (1980)). See text for more details.

be estimated from the  $t_3$  time through Schmidt-Kaler’s MMRD relation (Schmidt 1957):

$$M_{V,\max} = -11.75 + 2.5 \log t_3. \quad (3)$$

Then the distance is obtained from

$$(m - M)_{V,\max} = -5 + 5 \log d + 3.1E(B - V), \quad (4)$$

if  $E(B - V)$  is known. If we adopt  $t_3 = 5.3$  from the optical maximum of  $m_V = 5.4$  (Harrison & Stringfellow 1994), this equation gives  $M_V = -9.94$ . With the apparent visual magnitude of  $m_V = 5.4$  and  $E(B - V) = 0.53$ , we get  $d = 5.49$  kpc. If  $E(B - V)$  is not fixed, we have

$$(m - M)_{V,\max} = -5 + 5 \log d + 3.1E(B - V) = 15.34, \quad (5)$$

which is plotted in Figure 13 (labeled “MMRD1”).

The Schmidt-Kaler law (Eq. (3)) yields a bit larger magnitudes for a faster nova. Della Valle & Livio (1995) derived the following MMRD relation which is a good representation of fast novae,

$$M_{V,\max} = -7.92 - 0.81 \arctan \frac{1.32 - \log(t_2)}{0.23}. \quad (6)$$

For  $t_2 = 1.4$  (Harrison & Stringfellow 1994) this equation gives  $M_V = -9.04$ . With the apparent visual magnitude of  $m_V = 5.4$  and  $E(B - V) = 0.53$ , we get  $d = 3.6$  kpc. If  $E(B - V)$  is not fixed, we have

$$(m - M)_{V,\max} = -5 + 5 \log d + 3.1E(B - V) = 14.44, \quad (7)$$

which is plotted in Figure 13 (labeled “MMRD2”).

Another way to estimate the distance to V838 Her comes from comparing the observed light curve of 1455 Å band with the corresponding model fluxes (see Paper I, Paper III, and Kato & Hachisu 2005,

2007). We show that the calculated flux at  $\lambda = 1455 \text{ \AA}$  at a distance of 1 kpc for Model 2 is  $F_\lambda^{\text{mod}} = 6.6 \times 10^{-10} \text{ erg cm}^{-2} \text{ s}^{-1} \text{ \AA}^{-1}$  at the UV peak in Figure 7a. The corresponding observed peak flux is  $F_\lambda^{\text{obs}} = 1.57 \times 10^{-12} \text{ erg cm}^{-2} \text{ s}^{-1} \text{ \AA}^{-1}$ . From these values one obtains the following relation between distance and reddening:

$$m_\lambda^{\text{obs}} - M_\lambda^{\text{mod}} = 5 \log\left(\frac{d}{1 \text{ kpc}}\right) + A_\lambda E(B - V) = 6.56 \quad (8)$$

where  $m_\lambda = -2.5 \log(F_\lambda)$ , and  $A_\lambda = 8.3$  at  $\lambda = 1455 \text{ \AA}$  (Seaton 1979). This curve is reported in Figure 13, and is labeled “UV 1455Å”. Equation (8) provides a distance of  $2.7 \pm 0.5 \text{ kpc}$  for  $E(B - V) = 0.53 \pm 0.05$ . If we take the upper and lower values of the UV peak ( $1.57 \pm 0.20$ )  $\times 10^{-12} \text{ erg cm}^{-2} \text{ s}^{-1} \text{ \AA}^{-1}$ , we get the distance of 2.9 kpc and 2.5 kpc, respectively. This is however, an extreme case, because the fitting becomes much worse in Figure 7. Therefore, we estimate the distance to be  $2.7 \pm 0.5 \text{ kpc}$  for  $E(B - V) = 0.53 \pm 0.05$  from UV light curve fitting. Note that the distance hardly changes for all the models in Table 3.

One may estimate a lower limit for the distance assuming that the flux of free-free emission is larger than the blackbody flux in optical wavelength region. As the optical free-free flux is dominated by photons reprocessed from shorter wavelength photons of blackbody continuum, free-free flux is larger than that of corresponding blackbody emission at the optical wavelength during the early phase of nova outburst (Hauschildt et al. 1997). Our experience of light curve fitting also suggest that this condition is empirically satisfied in several novae (see Kato & Hachisu 2007, for V1974 Cyg). Thus, we assume this condition, which is written as

$$m_V - M_V = 5 \log\left(\frac{d}{10 \text{ pc}}\right) + 3.1E(B - V) > 13.2. \quad (9)$$

The shadowed region labeled “BB” in Figure 13 is where Equation (9) is not satisfied. The border gives the lower limit for the distance to V838 Her, which is  $d > 2.46 \text{ kpc}$  for the particular value of  $E(B - V) = 0.53$ .

As shown in Table 1, the distances in literature are very scattered. The distance obtained from MMRD tends to be larger than ours as shown in Figure 13. Starrfield et al. (1992) obtained a distance of  $\sim 3.4 \text{ kpc}$  and  $E(B - V) \sim 0.6$  from the comparison of total UV flux (LWP/SPW) including both of line and continuum emission with that of nova LMC 1991 showing a similar spectrum development. This is similar but contrasted to our method in the sense that we use only continuum emission around  $1455 \text{ \AA}$  and compare it with the theoretical value. Their value  $\sim 3.4 \text{ kpc}$  is larger than ours, but closer than other estimates using the MMRD relation.

#### 5.4. Emergence of the Companion

In the early phase of the outburst, the photosphere of the WD envelope extends beyond the size of the binary orbit. The companion is deeply embedded inside the WD photosphere. After maximum expansion, the photospheric radius shrinks owing to wind mass loss. We can estimate the epoch when the companion appears from the photosphere.

From Warner’s (1995) empirical formula the mass of the donor star (companion) is expressed as:

$$\frac{M_2}{M_\odot} \approx 0.065 \left(\frac{P_{\text{orb}}}{\text{hours}}\right)^{5/4}, \quad \text{for } 1.3 < \frac{P_{\text{orb}}}{\text{hours}} < 9 \quad (10)$$

which gives  $M_2 = 0.76 M_\odot$  for  $P_{\text{orb}} = 0.2976 \text{ days}$  (7.14 hr), in good agreement with the value  $M_2 = 0.73 - 0.75 M_\odot$  obtained by Szkody & Ingram (1994), although they could not well constrain the mass of the primary component ( $M_{\text{WD}} > 0.62 M_\odot$ ).

The binary separation is obtained from Kepler’s law to be  $a = 2.41 R_\odot$  for  $M_{\text{WD}} = 1.35 M_\odot$ . The effective radius of the Roche lobe is  $R_1^* = 1.0 R_\odot$  for the primary component (WD), and  $R_2^* = 0.80 R_\odot$  for the secondary. Here we use an empirical formula of  $R_1^*$  and  $R_2^*$  given by Eggleton (1983). In our model, the companion emerges from the WD envelope when the photospheric radius of the WD shrinks to  $R_{\text{ph}} \sim 3.2 R_\odot$  (the separation plus  $R_2^*$ ),  $\sim 2.4 R_\odot$  (the separation), or  $1.6 R_\odot$  (the separation minus  $R_2^*$ ). This occurs on day 7, 9 and 11, respectively, in our Model 2. The emergence time of the companion (the central time) is shown in Table 3 and also indicated by a small arrow in Figures 9, 10 and 11. As the eclipse is due to the occultation of the WD, or of the central part of the accretion disk by the companion, the eclipse must occur after the above three epochs of emergence. Our estimated time of companion emergence is a rough estimate, but it is well before the first eclipse observation (day 21), so consistent with observation.

#### 5.5. Mass determination from the duration of the 1455 Å maximum

The duration of a UV nova outburst, as measured by the full width at half maximum  $t_{\text{FWHM}}$  of the  $1455 \text{ \AA}$  light curve (Cassatella et al. 2002) is tightly correlated with the nova decay time  $t_3$  which, in turn, is a primary indicator of the WD mass (Livio 1992). Detailed model calculations by Hachisu & Kato (2006) have confirmed the primary dependence of  $t_{\text{FWHM}}$  on  $M_{\text{WD}}$  and have shown, in addition, that there is secondary, weaker, dependence on chemical composition. These results imply that the duration of a UV nova outburst can be used as a useful tool to estimate the WD mass in nova systems.

In Figure 14 we compare the theoretical relation of  $t_{\text{FWHM}}$  vs. WD mass (Hachisu & Kato 2006) with those obtained from the measured values of  $t_{\text{FWHM}}$  (Cassatella et al. 2002) and from the WD masses of seven classical novae, including V838 Her, estimated from the previous works (namely from Paper I for V1668 Cyg and V1974 Cyg; from Kato & Hachisu 2007) for V351 Pup, OS And and V693 CrA, and from this paper for V838 Her). We recall that the masses of these novae were determined by using the light-curve fitting method not only on the UV  $1455 \text{ \AA}$  light curve, but also on the optical, infrared, and supersoft X-ray light curves. For GQ Mus the UV data are very scattered so we plot here the theoretically fitted value in Paper III.

The largest possible error in this mass determination arises from ambiguity of chemical composition because observationally determined values are sometimes very scattered in literature. If we adopt different chemical composition, we get different  $M_{\text{WD}}$  even for the same  $t_{\text{FWHM}}$  as shown in Figure 14. In the case of V838 Her,

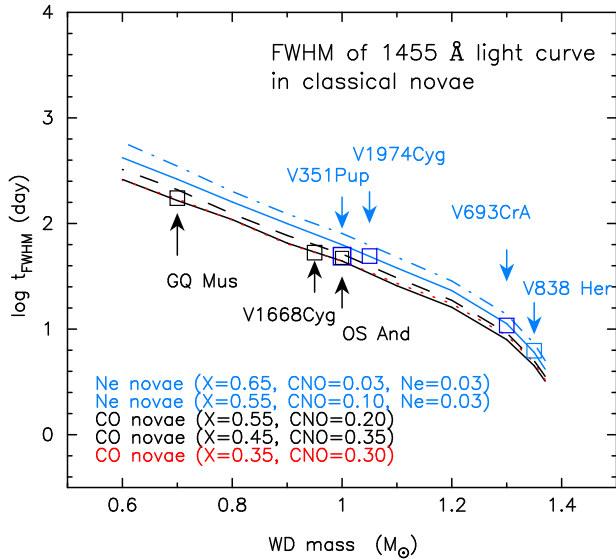


FIG. 14.— Duration (FWHM) of UV nova outburst at 1455 Å against the WD mass. *Dash-dotted line*: Neon novae ( $X = 0.65$ ,  $Y = 0.27$ ,  $X_{\text{CNO}} = 0.03$ ,  $X_{\text{Ne}} = 0.03$ ). *Top solid line*: Neon novae ( $X = 0.55$ ,  $Y = 0.30$ ,  $X_{\text{CNO}} = 0.10$ ,  $X_{\text{Ne}} = 0.03$ ). *Dashed line*: CO novae ( $X = 0.55$ ,  $Y = 0.23$ ,  $X_{\text{CNO}} = 0.20$ ). *Bottom solid line*: CO novae ( $X = 0.45$ ,  $Y = 0.18$ ,  $X_{\text{CNO}} = 0.35$ ). *Dotted line*: CO novae ( $X = 0.35$ ,  $Y = 0.33$ ,  $X_{\text{CNO}} = 0.30$ ) (almost overlapped with the lower solid line). We assume  $Z = 0.02$  for all the models. Arrows indicate the WD mass of individual novae. For V838 Her we adopt Model 2. For GQ Mus, we used the results in Paper III. For V1668 Cyg and V1974 Cyg, the results in Paper I. For V351 Pup, OS And and V693 CrA, the results in Kato & Hachisu (2007). Novae named in the upper side of the lines are Ne novae whereas those in the lower side are CO novae.

however, the difference of mass determination  $\Delta M_{\text{WD}}$  is relatively small, because in very massive WDs,  $t_{\text{FWHM}}$  quickly decreases and then strongly depends on the WD mass but weakly on the composition.

Another possible source of ambiguity in the determination of WD mass may come from effects of dust. Figure 15 compares the duration of UV nova outburst  $t_{\text{FWHM}}$ , as predicted by our models, with the observed values from Cassatella et al. (2002) for five novae. The figure shows that there is a reasonable agreement between the two sets of data, except the dust forming novae V1668 Cyg and OS And. In these two objects, dust formation took place shortly after the UV 1455 Å maximum, so making the measured  $t_{\text{FWHM}}$  significantly smaller than expected. In the case of V838 Her, in spite of being a dust forming nova, the mass of dust was too small to affect the UV light curve, as discussed in Section 5.2.

Note that the mass determination of our light curve analysis is based not only on the UV data fittings, but also on the optical and IR fittings, so the error in UV fitting does not directly reflect to the resultant  $M_{\text{WD}}$ .

Figure 14 indicates that less massive WDs ( $\lesssim 1 M_{\odot}$ ) are systematically CO-rich, while more massive WDs ( $\gtrsim 1 M_{\odot}$ ) are neon-rich. It has been argued that heavy element enrichment of nova ejecta is caused by dredge-up of WD core material so that, for example, C and O enrichment is an indication of a CO WD. An ONe WD is born in massive stars after ignition of a CO core and, therefore, ONe WDs are usually more massive than CO WDs when they are just born. Our results are consistent with this.

The mass boundary of CO WDs and ONe WDs are

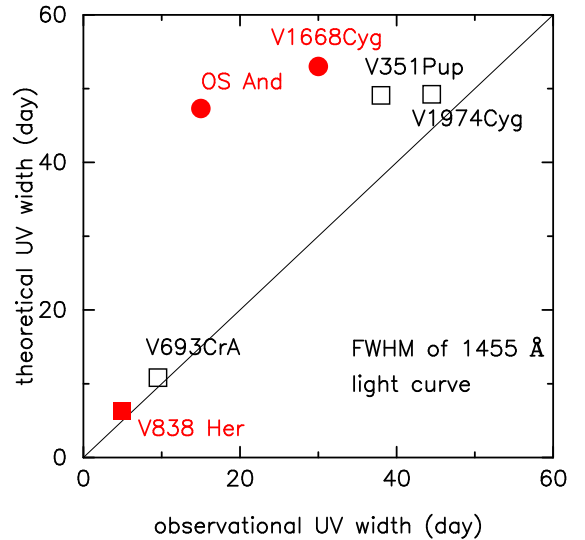


FIG. 15.— Observational and theoretical durations of the UV 1455 Å nova outbursts. Filled symbols (red) denote novae with dust formation. Squares and circles denote Ne and CO novae, respectively. Observational data are taken from Cassatella et al. (2002). The large deviation of OS And and V1668 Cyg is due to dust formation. See text for details.

suggested to be  $1.0\text{--}1.1 M_{\odot}$ . Iben (1990) summarized that a star of initial mass of  $5\text{--}10 M_{\odot}$  leaves a CO WD of mass  $0.75\text{--}1.1 M_{\odot}$  and a star of  $10\text{--}12 M_{\odot}$  becomes ONe WD. García-Berro et al. (1997) calculated stellar evolution of  $9 M_{\odot}$  star which finally becomes an  $\sim 1.08 M_{\odot}$  ONe core surrounded by an CO envelope of  $\sim 0.08 M_{\odot}$ . Umeda et al. (1999) calculated stellar evolution until CO core ignition with fine grid of initial stellar mass and concluded that the mass of CO WDs born in binaries is less massive than  $1.07 M_{\odot}$  of which initial mass is  $\sim 8 M_{\odot}$  for  $Z = 0.02$ . Meng et al. (2008) obtained CO core mass consistent with Umeda et al.'s value. These predictions are consistent with our results in Figure 14.

### 5.6. X-ray observations

X-ray emission from V838 Her has been detected with *ROSAT* as early as 5 days after the discovery (Lloyd et al. 1992; O'Brien et al. 1994), and was found to be consistent with emission from shocked plasma with  $T \sim 10$  keV (O'Brien et al. 1994). According to these authors the shock could originate from within the ejected material itself or by interaction of the ejecta with pre-existing circumstellar matter. In our Model 2 the optically thick wind lasts until day  $\sim 52$  days (see Table 3 for other models); this is consistent with the picture that the wind collides with circumstellar matter to produce the observed X-ray flux.

### 5.7. Quiescent Phase

The presence of an accretion disk has been suggested from the long duration of the eclipse (Ingram et al. 1992), and from the depth of eclipse at minimum (Leibowitz 1993).

The absolute magnitude of a disk, seen at an inclination angle  $i$ , is approximated by

$$M_V(\text{obs}) = -9.48 - \frac{5}{3} \log \left( \frac{M_{\text{WD}}}{M_{\odot}} \frac{\dot{M}_{\text{acc}}}{M_{\odot} \text{ yr}^{-1}} \right)$$

$$-\frac{5}{2} \log(2 \cos i), \quad (11)$$

where  $M_{\text{WD}}$  is the WD mass, and  $\dot{M}_{\text{acc}}$  is the mass accretion rate (Eq. (A6) in Webbink et al. 1987). Szkody & Ingram (1994) estimated the inclination of the disk to be  $i = 78 - 90^\circ$ . Assuming  $M_{\text{WD}} = 1.35 M_\odot$  and  $i = 80^\circ$ , we get  $M_V = 6.5, 4.8,$  and  $3.1$  for the mass accretion rates of  $1 \times 10^{-9}, 1 \times 10^{-8},$  and  $1 \times 10^{-7} M_\odot \text{ yr}^{-1}$ , respectively. The corresponding apparent magnitudes, as calculated from equation (4) with  $E(B - V) = 0.53$  and  $d = 2.7 \text{ kpc}$  are  $m_V = 20.3, 18.6$  and  $16.9$ . Considering the ambiguity of assumed accretion rates and the inclination angle, these values are consistent with the preoutburst magnitude reported in Section 1.

The contribution of a companion star to the quiescent luminosity is estimated as follows. Patterson (1984) gives an empirical relation between the absolute magnitude of a Roche lobe filling companion and its orbital period as

$$M_V = 22 - 17.46 \log P(\text{hr}), \quad (12)$$

for  $0.7 < \log P(\text{hr}) < 1.1$ . For  $P(\text{hr}) = 7.14 \text{ hr}$  (Ingram et al. 1992; Leibowitz et al. 1992) we get  $M_V = 7.1$  and  $m_V = 20.6$ . Thus, the companion star would be fainter than the accretion disk although there are ambiguity in the mass accretion rate and the inclination angle. This is also consistent with a faint companion suggested from a small upper limit of  $\sim 0.05 \text{ mag}$  on the depth of the secondary minimum (Leibowitz

1993) and from no visible evidence in the spectrum (Szkody & Ingram 1994).

## 6. CONCLUSIONS

We have applied the 'universal decline law' of classical novae described in §3.3 to one of the fastest novae V838 Her and derived various parameters. Our main results are summarized as follows:

1. An analysis of the *IUE* reprocessed data of V838 Her indicates  $E(B - V) = 0.53 \pm 0.05$ .
2. The  $1.35 \pm 0.02 M_\odot$  WD model reasonably reproduces the light curves of V838 Her both in the optical and in the UV 1455 Å band as well as in the infrared *H* and *K* bands at the early stages, until dust formation takes place. Model 2 in table 3 is the best fit model.
3. The distance is estimated to be  $d \sim 2.7 \pm 0.5 \text{ kpc}$  from the UV 1455 Å light curve fitting.
4. We have estimated ejecta mass  $\Delta M_{\text{wind}} \sim (2 - 3) \times 10^{-6} M_\odot$  lost by winds.

The authors are grateful to Takashi Iijima for fruitful discussion, and also to an anonymous referee for useful comments to improve the manuscript. We also thank the American Association of Variable Star Observers (AAVSO) for the visual data of V838 Her. This research has been supported in part by the Grant-in-Aid for Scientific Research (20540227) of the Japan Society for the Promotion of Science.

## APPENDIX

Figure 16 demonstrates a "universality" of nova light curves, in which five classical novae are shown in the visual (*V* and *y*) and UV 1455 Å band (except V1500 Cyg: no UV 1455 Å band is available). Each peak of the UV 1455 Å flux is normalized in order to match the peak of V838 Her. Also, the time-scale of each nova is normalized so that each UV 1455 Å light curve is overlapped with that of V838 Her. The same normalizing factor of time-scale is applied to both the UV and the optical light curves. These normalizing factors, obtained by eye fitting, are summarized in the figure caption.

Our universal decline law predicts that the light curves, normalized in this way, should merge into one, independent of the WD mass and chemical composition (see Paper I). This match is excellent for the *y* light curve, because this band is little contaminated by strong emission lines (Hachisu et al. 2008). As one may appreciate from the figure, there is a good overlap between the light curves of V1668 Cyg (*y*-magnitude, connected by solid line), V1500 Cyg (*y*-magnitude), and the initial phase of V1974 Cyg (*V* magnitude). It also appears from the figure that, whenever strong emission lines provide the dominant contribution to the magnitude, the data deviate above the V1668 Cyg line. In the case of V838 Her the data are scattered compared with the above three objects, therefore, we fit its lowest boundary of the data with the V1668 Cyg line. We can see excess of the visual magnitudes between day 3 and day 6.

Four UV 1455 Å light curves also show a good agreement with each other, although V1668 Cyg shows a drop at 0.37 in the normalized time due to dust formation (Gehrz et al. 1980). We don't see any indication of sharp drop like this in V838 Her.

## REFERENCES

- Alcock, G. 1991, IAU Circ., No. 5222  
 Cassatella, A., Altamore, A., & González-Riestra, R. 2002, *A&A*, 384, 1023  
 Cassatella, A., Altamore, A., & González-Riestra, R. 2005, *A&A*, 439, 205  
 Cassatella, A., González-Riestra, R., & Selvelli, P. 2004a, INES Access Guide No.3 Classical Novae (ESA: Netherlands)  
 Cassatella, A., Lamers, H. J. G. L. M., Rossi, C., Altamore, A., & González-Riestra, R. 2004b, *A&A*, 420, 571  
 Chandrasekhar, T., Ashok, N.M., & Ragland, S. 1992, *MNRAS*, 255, 412  
 Della Valle, M., & Livio, M. *ApJ*, 452, 704  
 Eggleton, P.P. 1983, *ApJ*, 268, 368  
 Evans, A. et al. 2003, *AJ*, 126, 1981  
 García-Berro, E., Ritossa, C., & Iben, I. Jr. 1997, *ApJ*, 485, 765  
 Gehrz, R.D., Hackwell, J.A., Grasdalen, G.L., Ney, E.P., Neugebauer, G., and Sellgren, K. 1980, *ApJ*, 239, 570  
 Grevesse, N., & Anders, E. 1989, *Cosmic Abundances of Matter*, ed. C. J. Waddington (New York: AIP), 1  
 Groenewegen, M. A. T., & Lamers, H. J. G. L. M. 1989, *A&AS*, 79, 359  
 Hachisu, I., & Kato, M. 2006, *ApJS*, 167, 59 (Paper I)  
 Hachisu, I., & Kato, M. 2009, *ApJ*, 694, L103-L106  
 Hachisu, I. et al. 2006, *ApJ*, 651, L141  
 Hachisu, I., Kato, M., & Cassatella, A. 2008, *ApJ*, 687, 1236 (Paper III)

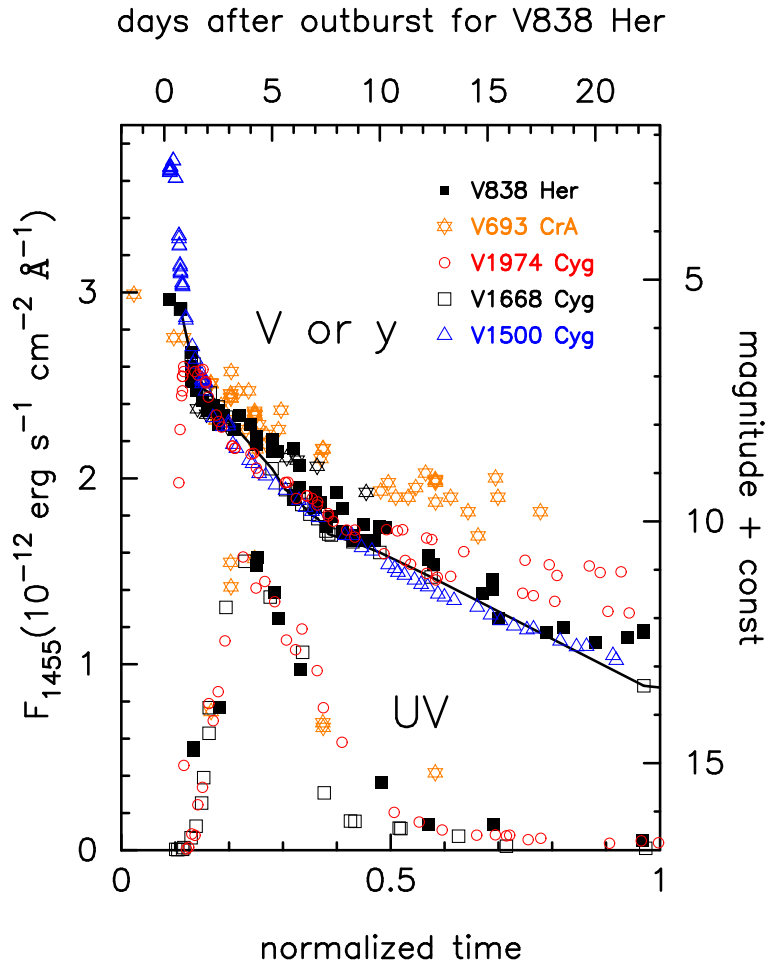


FIG. 16.— Scaling of five nova light curves. The observed light curve of classical novae, V693 CrA, V1974 Cyg, V1668 Cyg, and V1500 Cyg are overlapped to that of V838 Her. For V838 Her only the optical data in IAU Circulars and *IUE*  $V_{FES}$  data are shown. Optical data are  $y$  magnitudes for V1668 Cyg (connected by a solid line) and V1500 Cyg,  $V$  for V1974 Cyg (for the references, see Paper I),  $V$  and visual for V693 CrA (Kato & Hachisu 2007). The scale for the UV Flux (on the left-hand side), the magnitude, and the time after outburst refer to V838 Her. The scale of the other novae is normalized as follows: the upper limit in the UV flux scale (in  $\text{erg s}^{-1}\text{cm}^{-2}\text{\AA}^{-1}$ ), the lower limit in the magnitude, the upper limit in the magnitude, and the time normalized to unity (abscissa) have been set to: ( $3.9\text{E}-12$ , 16.8, 1.8, 25) for V838 Her, ( $1.9\text{E}-12$ , 18, 3, 54) for V693 CrA, ( $4.4\text{E}-11$ , 14.8,  $-0.2$ , 202) for V1974 Cyg, ( $4\text{E}-12$ , 18, 3, 200) for V1668 Cyg, and (no data, 16.1, 1.1, 162.8) for V1500 Cyg.

Hachisu, I., Kato, M., & Luna, G.J.M. 2007, *ApJ*, 659, L153  
Hachisu, I., Kato, M., & Nomoto, K. 1999a, *ApJ*, 522, 487  
Harrison, T.E. & Stringfellow, G.S. 1994, *ApJ*, 437, 827  
Hauschildt, P. H., Shore, S. N., Schwarz, G. J., Baron, E., Starrfield, S., & Allard, F. 1997, *ApJ*, 490, 803  
Humphreys, R.M., Zumach, W., & Stockwell, T. 1991 IAU Circ.No. 5224  
Iben, I., Jr. 1990 in *Confrontation between stellar pulsation and evolution*, ed. C. Cacciari, & G. Clementini, ASP Conf. Proc. (San Francisco, ), 11, 483  
Iijima, T., Cassatella, A., Kato, M., & Hachisu, I. 2009, *A&A*, in preparation  
Iglesias, C. A., & Rogers, F. J. 1996, *ApJ*, 464, 943  
Ingram, D., Garnavich, P., Green, P., & Szkody, P. 1992, *PASP*, 104, 402  
Kato, M. 1983, *PASJ*, 35, 507  
Kato, M. 1997, *ApJS*, 113, 121  
Kato, M. 1999, *PASJ*, 51, 525  
Kato, M., & Hachisu, I., 1994, *ApJ*, 437, 802  
Kato, M., & Hachisu, I., 2005, *ApJ*, 633, L117  
Kato, M., & Hachisu, I. 2007, *ApJ*, 657, 1004  
Kato, T., & Hirata, R. 1991 IAU Circ.No. 5262  
Kato, M., Hachisu, I., Kiyota, S., & Saio, H., 2008, *ApJ*, 684, 1366  
Kidger, M.R. & Martinez-roger, C. 1993, *A&A*, 267, 111  
Krautter, J., Ögelman, H., Starrfield, S., Wichmann, R., & Pfeffermann, E. 1996, *ApJ*, 456, 788

Lamers, H. J. G. L. M.; Cerruti-Sola, M.; Perinotto, M. 1987, *ApJ*, 314, 726  
Leibowitz, E. M., Mendelson, H., & Mashal, E. 1992, *ApJ*, 385, 49  
Leibowitz, E. M. 1993, *ApJ*, 411, L29  
Lloyd, H.M., O'Brien, T.J., Bode, M.F., Predehl, P., Schmitt, J.H.M.M., Trümper, J., Watson, M.G., & Pounds, K.A. 1992, *Nature*, 356, 222  
Lynch, D. K., Hackwell, J.A., & Russell, R. W. 1992, *ApJ*, 398, 632  
Matheson, T., Filippenko, A.V., & Ho, L.C. 1993, *ApJ*, 418, L29  
Meng, X., Chen, X., & Han, Z. 2008, *A&A*, 487, 625  
Neckel, Th., & Klare, G. 1980, *A&AS*, 42, 251  
Ness, J.-U., Schwarz, G. J., Retter, A., Starrfield, S., Schmitt, J. H. M. M., Gehrels, N., Burrows, D., & Osborne, J. P. 2007a, *ApJ*, 663, 505  
O'Brien, T.J., Lloyd, H.M., & Bode, M.F. 1994, *MNRAS*, 271, 155  
Orio, M., Covington, J., Ögelman, H. 2001, *A&A*, 373, 542  
Patterson, J. 1984, *ApJS*, 54, 443  
Politano, M., Starrfield, S., Truran, J.W. Weiss, A., & Sparks, W.M. 1995, *ApJ*, 448, 807  
Priyalnik, D. 1986, *ApJ*, 310, 222  
Priyalnik, D., & Kovetz, A. 1995, *ApJ*, 445, 789  
Schmidt, Th. 1957, *Z. Astrophys.*, 41, 181  
Schwarz, G.J., Shore, S. N., Starrfield, S., & Vanlandingham, K. M. 2007, *ApJ*, 657, 453  
Seaton, M. J. 1979, *MNRAS*, 187, 73

- Smith, C.H., Aitken, D.K., Roche, P.F., & Wright, C.M. 1995, MNRAS, 277, 259
- Sugano, M. 1991, IAU Circ., No. 5222
- Stickland, D. J., Penn, C. J., Seaton, M. J., Snijders, M. A. J., & Storey, P. J. 1981, MNRAS, 197, 107
- Starrfield, S., Shore, S. N., Sparks, W.M., Sonneborn, G., Truran, J.W., & Politano, M. 1992, ApJ, 391, L71
- Szkody, P. & Hoard, D.W. 1994, ApJ, 429,857
- Szkody, P. & Ingram, D. 1994, ApJ, 420,830
- Ueta, E. 1991, IAU Circ., No. 5265
- Umeda, H., Nomoto, K., Yamaoka, H., & Wanajo, S. 1999, ApJ, 513, 861
- Vanlandingham, K. M., Starrfield, S., & Shore, S. N. 1997, MNRAS, 290, 87
- Vanlandingham, K. M., Starrfield, S., Wagner, R. M., Shore, S. N., & Sonneborn, G. 1996, MNRAS, 282, 563
- West, R. M., 1991, IAU Circ.No. 5224
- Webbink, R.F., Livio, M., Truran, J.W., & Orio, M. 1987, ApJ, 314, 653
- Williams, R.E., Phillips, M.M., & Hamuy, M. 1994, ApJS, 90,297
- Woodward, C.E., Gehrz, R.D, Jones, T.J., & Lawrence, G.F. 1992, ApJ, 384, L41